Hydrogen oxidation kinetics on platinum-palladium bimetallic thin films for solid acid fuel cells

Haemin Paik, Andrey V. Berenov, Stephen J. Skinner, and Sossina M. Haile

Citation: APL Materials **7**, 013201 (2019); doi: 10.1063/1.5050093
View online: https://doi.org/10.1063/1.5050093
View Table of Contents: http://aip.scitation.org/toc/apm/7/1
Published by the American Institute of Physics

Hydrogen oxidation kinetics on platinum-palladium bimetallic thin films for solid acid fuel cells

Cite as: APL Mater. 7, 013201 (2019); doi: 10.1063/1.5050093
Submitted: 27 July 2018 • Accepted: 2 September 2018 •
Published Online: 6 December 2018

Haemin Paik,[1] Andrey V. Berenov,[2] Stephen J. Skinner,[2] and Sossina M. Haile[1,3,a)]

AFFILIATIONS

[1] Materials Science, California Institute of Technology, 1200 California Blvd., Pasadena, California 91125, USA
[2] Department of Materials, Imperial College London, Exhibition Road, London SW7 2AZ, United Kingdom
[3] Department of Materials Science and Engineering, Northwestern University, 2220 Campus Drive, Evanston, Illinois 60208, USA

[a)] **Author to whom correspondence should be addressed:** sossina.haile@northwestern.edu.

ABSTRACT

Solid acid fuel cells (SAFCs) based on the proton-conductive electrolyte CsH_2PO_4 have shown promising power densities at an intermediate operating temperature of ~250 °C. However, Pt loadings in SAFCs remain higher than desirable, and the electrocatalysis mechanisms in these devices are still unknown. Here, hydrogen oxidation kinetics on Pt and Pt-Pd bimetallic thin film electrodes on CsH_2PO_4 have been evaluated to establish the potential for a beneficial role of Pd in SAFC anodes. Symmetric cells fabricated by depositing a metal film on both sides of electrolyte discs are characterized for studying hydrogen electro-oxidation across the gas|metal|CsH_2PO_4 structure. It was found that Pd reacts with CsH_2PO_4, forming palladium phosphide at the metal-electrolyte interface. Accordingly, the activity of Pd was examined in a bilayer geometry of Pd|Pt|CsH_2PO_4|Pt|Pd. The bilayer Pt|Pd films showed much higher activity for hydrogen electro-oxidation than films of Pt alone, as measured by AC impedance spectroscopy. *Ex situ* low energy ion scattering and scanning transmission electron microscopy revealed that Pd diffused into the Pt layer under operating conditions. The dramatic impact of Pd along with its presence throughout the film suggests that it catalyzes reactions at both the metal-gas and metal-electrolyte interfaces, as well as increasing hydrogen diffusion rates through the films.

Fuel cells convert chemical energy into electrical energy through the electrochemical reaction of oxygen with a fuel such as hydrogen. Intermediate temperature fuel cells functioning at 200-500 °C combine the benefits of high temperature operation, such as fuel flexibility and high efficiency, with the advantages of low temperature operation including inexpensive auxiliary components and easy on-off cycling. Solid acid fuel cells (SAFCs) have drawn attention for their operability at intermediate temperature using the non-toxic, proton-conducting electrolyte, cesium dihydrogen phosphate (CsH_2PO_4).[1,2] At 250 °C CsH_2PO_4 displays high proton conductivity, ~10^{-2} S/cm, good stability, and high fuel cell power density.[3,4] While many of the performance characteristics of SAFCs are now approaching commercial requirements, market entry has been hampered in large part by high Pt loadings (~2 mg_{Pt}/cm^2 for both electrodes combined). Moreover, surprisingly few alternatives to Pt have emerged for either the hydrogen oxidation reaction or the oxygen reduction reaction in SAFCs.

In the present work, we examine the suitability of Pd as a catalyst component in SAFC anodes. Pd and Pd-Pt alloys have shown high activity in SAFC cathodes, but these materials quickly react with the electrolyte.[5–7] It has been suggested that this reaction is enabled by the ready oxidation of Pd in the SAFC cathode environment. By contrast, no such oxidation

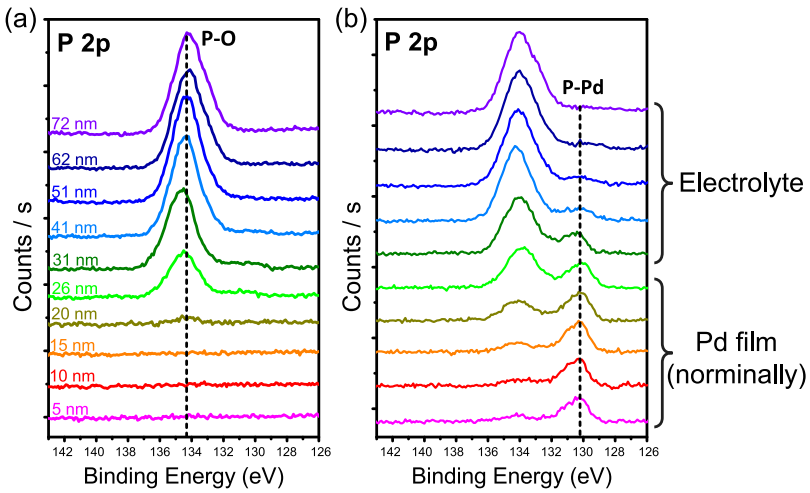

FIG. 1. X-ray photoelectron spectroscopy (XPS) depth profile analysis in the P 2p region, collected from Pd (30 nm) on CsH_2PO_4: (a) as-deposited and (b) after annealing for ~40 h under SAFC anode conditions (T = 248 °C, pH_2 = 0.6 atm, pH_2O = 0.4 atm). The etching depth indicated in (a) applies also to (b). Although not easily seen here, P 2p has spin-orbital doublets with a difference of 0.9 ± 0.1 eV between p1/2 and p3/2.

reaction would be expected in the anode environment, suggesting the possibility of stability of Pd^0 against reaction with CsH_2PO_4. Measurements of Pd electrocatalytic activity for hydrogen oxidation in SAFC anodes, however, have produced contradictory results. Louie *et al.*[8] and Sasaki[9] independently found Pd to be much more active than Pt, whereas Papandrew *et al.*[10] have reported that Pt and Pd are comparable in terms of both activity and stability. In the present work, we examine the reactivity of Pd with CsH_2PO_4 under anode conditions and explore strategies for using Pd to enhance hydrogen electro-oxidation rates in solid acid systems. To facilitate interpretation of electrochemical behavior, we employ a thin film geometry in which metal films are deposited onto a polycrystalline disk of the CsH_2PO_4 electrolyte, and the resulting symmetric cells are examined under a uniform hydrogen-rich gas.[8,11–13]

For evaluation of possible reactivity between Pd and CsH_2PO_4 under SAFC anode conditions, we performed depth-resolved X-ray photoelectron spectroscopy (XPS) on as-prepared and annealed Pd-film|CsH_2PO_4 structures, Fig. 1. The heat treatment was carried out at 250 °C under humidified H_2 (pH_2O = 0.4 atm, balance H_2) for 40 h. The as-prepared structure is well-behaved, showing, for example, the presence of a component in the P 2p edge region at 134.5 ± 0.1 eV corresponding to the P—O bonds in CsH_2PO_4, only after the Pd film has been removed. The emergence of the P—O peak at a nominal depth of 26 nm despite a film that is 30 nm thick is likely due to the 5 nm sampling depth inherent to the XPS method. The spectra from the annealed structure, by contrast, reveal the presence of P through the entirety of the nominally Pd film with a peak position of 130.1 ± 0.1 eV. This feature corresponds to the formation of palladium phosphide[14] and reveals that even metallic Pd can react with CsH_2PO_4. Deeper into the structure, the P 2p peak position corresponds to that in pristine CsH_2PO_4. A large region (~50 nm) of coexistence between reduced and oxidized phosphorous suggests a non-uniform reaction front.

The XPS spectra about the Pd 3d and Cs 3d peaks, Fig. S1 of the supplementary material, were consistent with the interpretation developed on the basis of the P 2p spectra. The Pd film and CsH_2PO_4 electrolyte are sharply delineated in the as-prepared sample, whereas after annealing, Pd is incorporated into the electrolyte, and conversely, Cs is incorporated into the film. Further evidence of reaction between Pd and CsH_2PO_4 is provided from electron microscopy imaging of free-standing films obtained by dissolving away the CsH_2PO_4 substrate, Fig. 2. The as-deposited films reveal the surface structure of the underlying polycrystalline electrolyte. By contrast, the annealed films have evolved into a less-defined structure with significant porosity. Such porosity presumably contributes to the detection by XPS of P and Cs even at the very top region of the annealed CsH_2PO_4-Pd structure,

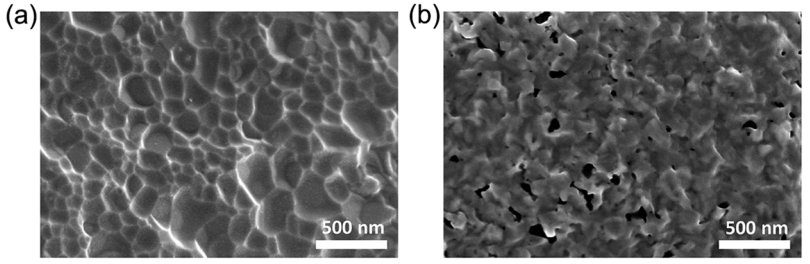

FIG. 2. Scanning electron microscope (SEM) images of the electrolyte-facing side of freestanding 30 nm Pd films removed from the CsH_2PO_4 substrate: (a) as deposited and (b) after annealing for ~40 h under SAFC anode conditions (T = 248 °C, pH_2 = 0.6 atm, pH_2O = 0.4 atm). Image in (a) reflects the morphology of the polycrystalline substrate and is essentially identical of that of analogous Pt films, Fig. S2 and prior work.[11]

Fig. 1(b) and Fig. S1(d) of the supplementary material. Moreover, the XPS analysis of the annealed free-standing Pd films revealed the presence of significant quantities of P and Cs on the electrolyte-facing side, whereas no P or Cs was detected in films which had not been annealed, Fig. S2 of the supplementary material. A similar study of freestanding Pt films showed no morphological evolution in response to heat treatment and no evidence of P or Cs incorporation, Figs. S3 and S4 of the supplementary material.

Based on these observations, the overall reaction between CsH_2PO_4 and Pd is tentatively described as

$$CsH_2PO_4 + Pd + zH_{2(g)} \rightarrow \tfrac{1}{2}Cs_2O/CsOH + PdxP + yH_2O_{(g)},$$

with Cs remaining in the fully oxidized state, whether it exists in the electrolyte or is part of a minor impurity phase in the metal/metal phosphide film. A slight shift in the Pd peak position after annealing toward high binding energy at the metal-electrolyte interface [Figs. S1(b) and S2(c) of the supplementary material] indicates maximum formation of the phosphide at this location.

In light of the obvious reaction between CsH_2PO_4 and Pd, electrochemical experiments with Pd directly applied to the electrolyte material were not pursued. Instead, the activity of Pd for catalyzing the reaction step at the metal|gas interface was assessed using bilayer films of Pd on Pt, under the hypothesis that Pt would serve as a reaction barrier to be eventually replaced by a less expensive material should Pd prove promising in this configuration. In this context, it is to be noted that we have previously demonstrated that the global interfacial impedance associated with hydrogen electro-oxidation across the CsH_2PO_4|Pt-film|gas interface as measured by AC impedance spectroscopy occurs via a serial process in which hydrogen is incorporated at the gas-metal interface, diffuses through the metal to the electrolyte interface, and is incorporated there as protons.[11] Though not demonstrated, it is supposed that charge transfer (conversion of atomic hydrogen to protons) occurs at the metal-electrolyte interface. In thick films (>~50 nm), the process is dominated by solid state diffusion through the Pt film, whereas the process is co-limited by reaction and diffusion across thinner films. On the basis of the film thickness trend, the resistance associated with the reaction step (or steps) alone, i.e., excluding diffusion, for hydrogen electrooxidation on Pt was estimated to be 2.2 Ω cm^2. Those results are generally corroborated here, Fig. S5 of the supplementary material, in which impedance as a function of the Pt film thickness in the range 15–80 nm has been recorded.

Because the diffusion and surface reaction resistance contributions to the global reaction resistance are known for Pt, it is possible to estimate the minimum resistance that would be encountered should a Pd overlayer render the reaction steps on Pt essentially barrierless. Of course, higher impedance than this minimum would result if Pd either has no effect or hampers the reaction steps. In Fig. 3(a) is shown a comparison of the measured global electrochemical resistance on Pt of varying thickness, the estimated minimum possible resistance values, and the measured resistance of Pt films with a 5 nm Pd overlayer. Impedance spectra were collected continuously under humidified hydrogen at 248 °C, and the results shown are from measurements made after 22 h of stabilization. The impedance drifted upwards over this period, Fig. S6 of the supplementary material, and the measurement after 22 h is taken as a reasonable equilibration time for the purpose of exploring the impact of the film thickness and bilayer structure. In all cases, the bilayer films display resistance values that are far lower than the estimated minimum resistances under the assumption that the role of the Pd is simply to eliminate the resistance associated with surface reaction steps. The result is particularly dramatic in the case of the 80 nm thick Pt film, which in principle, is entirely dominated by bulk diffusion resistance. Moreover, the thickness of the Pd overlayer has limited impact on the interfacial resistance. For an underlying Pt film that is 30 nm thick, the interfacial resistances fall from an already low value of ~0.6 Ω cm^2 when the Pd overlayer is 2 nm thick to ~0.2 Ω cm^2 when the thickness is 20 nm, Fig. 3(b).

The dramatic influence of Pd in the bilayer configuration indicates that it must modify the bulk characteristics of the underlying Pt. The behavior also suggests the possibility that Pt-Pd alloys may yield anodes with decreased precious metal loadings and higher activity than today's state-of-the-art electrodes. For example, given an electrode resistance of ~0.2 Ω cm^2 for bi-layer films of 30 nm Pt + 20 nm Pd, Fig. 3(b), with a total metal loading of ~0.09 mg/cm^2, the mass

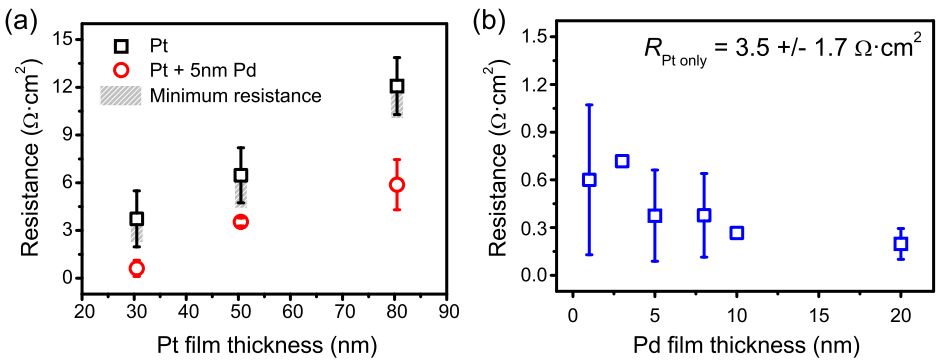

FIG. 3. Electrochemical interfacial resistance under SAFC anode conditions (T = 248 °C, pH_2 = 0.6 atm, pH_2O = 0.4 atm, after 22 h of equilibration) at zero bias of (a) Pt|CsH_2PO_4|Pt and Pd|Pt|CsH_2PO_4|Pt|Pd symmetric cells with varied Pt thickness and (b) Pd|Pt|CsH_2PO_4|Pt|Pd symmetric cells with varied Pd thickness on 30 nm Pt. Also shown in (a) is the resistance anticipated if only diffusion through the Pt film were to contribute to the measurement.

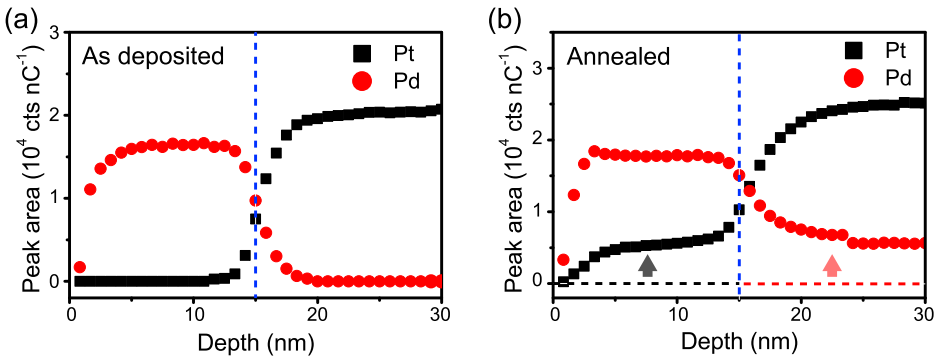

FIG. 4. Integrated Pd and Pt peak areas from low-energy ion scattering (LEIS) spectra as a function of depth, from 15 nm Pd|20 nm Pt bilayers on an Si substrate: (a) as deposited and (b) after annealing at 250 °C for 24 h in synthetic air. The interface between the Pd and Pt films is indicated with a dashed line in both figures.

normalized activity is on the order of 55 S/mg, a value approaching that achieved using Pt nanoparticles deposited on carbon nanotubes.[15]

The bulk phase diagram of the Pt-Pd system suggests limited miscibility of these elements at 250 °C,[16] but the data are not entirely conclusive. The clear impact of Pd on the bulk characteristics of Pt films motivated us to perform chemical analysis of Pd-Pt bilayer films and search for possible intermixing. Specifically, as-deposited and annealed bilayer structures were characterized using depth-resolved low energy ion scattering (LEIS) spectroscopy, where depth profiling was achieved using Ar sputtering, and cross-sectional energy dispersive spectroscopy (EDS) in combination with high resolution scanning transmission electron microscopy (STEM). For ease of interpretation, the analyses were performed on bilayers grown on single crystal Si (111) with Pt and Pd thicknesses of 20 nm and 15 nm, respectively, and high temperature annealing was performed under dry air. Both the LEIS and EDS, Figs. 4 and 5, respectively, show that the as-deposited bilayers are formed of distinct Pd and Pt films. Depletion of Pd at the top surface suggested by the LEIS measurements, Fig. 4(a), is likely due to the presence of exterior impurities, and an apparent intermixing region of ~5 nm at the Pd-Pt interface is likely due to roughness created by the Ar sputtering.[17] After exposure to 250 °C for 24 h, by contrast, Pt is clearly detected in the Pd region and conversely, Pd is clearly detected in the Pt region, Figs. 4(b) and 5(b).

Complete intermixing between Pd and Pt is unexpected in light of the limited miscibility of these two metals at 250 °C. However, it is known that when a polycrystalline metal film is in contact with another material, rapid incorporation of the foreign element along grain boundaries can occur even at a low temperature.[18] The heterogeneous distribution of Pt in Pd and of Pt in Pd as evidenced by the EDS elemental mapping, Fig. 5(b), suggests that such a phenomenon has occurred here. Accordingly, we propose that Pd-rich grain boundaries within the nominally Pt film become pathways for rapid hydrogen diffusion, Fig. 6. With increasing thickness of the underlying Pt film at constant Pd thickness, the cross-sectional area of such Pd-rich pathways must decrease, resulting in the observed increase in the global electrochemical reaction resistance, Fig. 3(a). The analogous situation presumably occurs when the thickness of the Pd film is varied at a fixed Pt thickness, Fig. 3(b). The extremely low impedance (0.2-0.5 Ω cm^2) when the Pd:Pt film thickness ratio exceeds 2:30, falling below that for the electrochemical reaction step(s) of Pt-only films (~2.2 Ω cm^2), indicates that Pd must also provide benefit to the interfacial processes.

In an attempt to assess whether the benefits of Pd accrue from the inherent chemistry of a fine-scale composite of Pt-Pd or from the proposed grain-boundary templated structure, we measured the electrochemical characteristics of co-sputtered films of Pd and Pt. Remarkably, the co-sputtering yields resistance values that are about 3 times greater than that of bilayer structures with identical overall composition and film thickness, Fig. 7. The result supports the hypothesis that grain-boundary templating creates favorable hydrogen transport pathways. Despite the activity penalty encountered by co-sputtering, even these films show

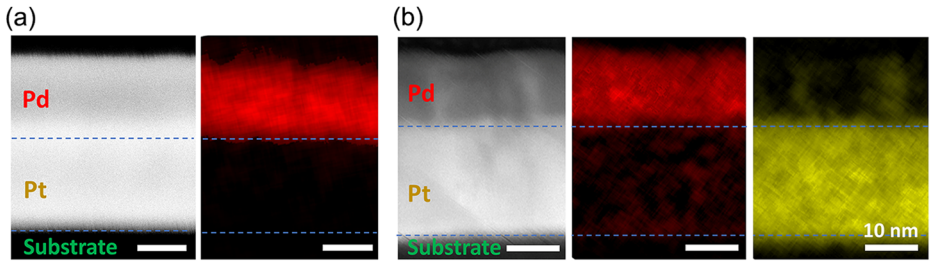

FIG. 5. Scanning transmission electron microscope (STEM) images in the high-angle annular dark-field (HAADF) mode and energy-dispersive X-ray spectroscopy (EDS) measurements of Pd (red) and Pt (yellow) concentrations, from 15 nm Pd|20 nm Pt bilayers on an Si substrate: (a) as-deposited and (b) after annealing at 250 °C for 24 h in synthetic air.

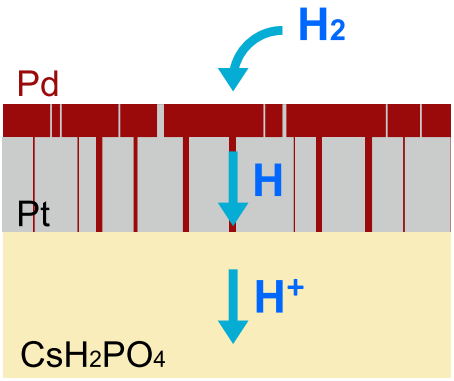

FIG. 6. Schematic of the structure proposed to form from Pt-Pd bilayers as a consequence of Pt-Pd interdiffusion along grain boundaries and the resulting pathways created for hydrogen electrooxidation on CsH_2PO_4.

much higher activity than Pt-only films of equal thickness and even higher activity than if only the surface steps on Pt are considered.

In summary, despite reaction between Pd and CsH_2PO_4 under reducing conditions, Pd-Pt nanocomposites appear to be more suitable electrocatalysts for hydrogen electrooxidation than Pt alone in solid acid fuel cells. Moreover, we find that the activity in such composites can be manipulated via control of the Pd-Pt distribution. We propose that Pd in an initially bilayered structure is incorporated into the grain boundaries of Pt films, creating pathways for rapid hydrogen diffusion. Remarkably, the surface/interfacial reaction steps in such composite films are also more facile than the analogous steps on Pt-only films. This observation opens up the possibility that the products of reaction between Pd and CsH_2PO_4, which require several hours to form and may have been overlooked in other experiments, may be highly active catalysts for hydrogen electrooxidation.

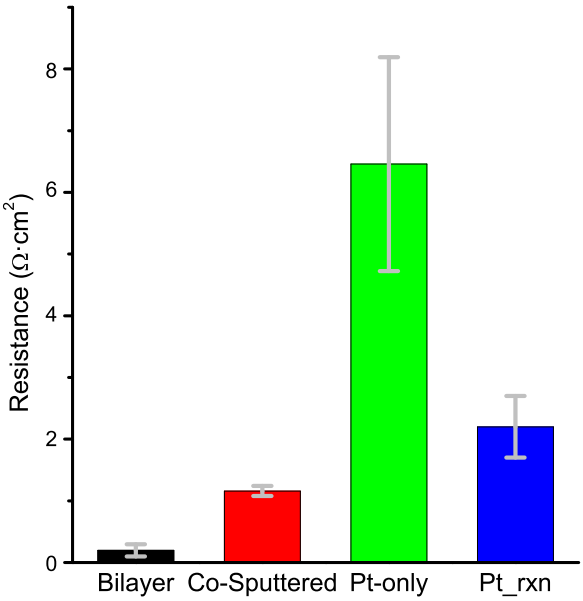

FIG. 7. Comparison of electrode resistance under hydrogen at 250 °C obtained from different types of 50 nm thick films on CsH_2PO_4: Pd-20nm|Pt-30nm; co-sputtered Pd_2Pt_3; Pt; and an estimate of the resistance for the surface reaction steps (only) on Pt. Error bars are the standard deviations obtained from averaging results from multiple cells.

CsH_2PO_4 was synthesized by dissolving Cs_2CO_3 and H_3PO_4 (85% assay) in de-ionized water, followed by precipitation in methanol. Disks of CsH_2PO_4, 0.75 in. diameter and typically 1 mm in thickness, were fabricated by uniaxial compression at 69 MPa. The surfaces were polished to a final mirror finish using silicon carbide sandpaper with a grit size of 8.4 μm. Metal deposition was performed using an AJA International ATC Orion system under 3 mTorr Ar. Pt was deposited in the DC mode using a plasma power of 75 W, and Pd in the RF mode using a power of 150 W.

X-ray diffraction patterns were collected using a Rigaku SmartLab X-ray diffractometer (Cu Kα radiation). Diffraction analysis was used to confirm synthesis of CsH_2PO_4 and deposition of crystalline metal films (not shown). Field emission scanning electron microscopy (FE-SEM) was performed using Hitachi SU8030 with accelerating voltage 5 kV. XPS spectra were measured with a Thermo Scientific ESCALAB 250Xi X-ray photoelectron spectroscopy system using Al Kα X-ray radiation in combination with an electron flood gun. The X-ray probe size was 300 μm. For depth profiling, Ar^+ ion with 3 keV energy was used to etch 2 × 2 mm^2 area of the sample. All spectra were referenced to the C 1s peak (284.8 eV).

Low-energy ion scattering (LEIS) experiments were performed using a Qtac100 (ION-TOF GmbH, Germany) instrument fitted with a double toroidal energy analyzer, which collects the scattered ions at a scattering angle of 145° from all azimuthal angles. The LEIS spectra were collected using 3 keV He^+ primary ion beams directed perpendicular to the sample surface. The primary beam was rastered over a large area (1.0 × 1.0 mm^2) to maintain an ion fluence below 10^{15} ions cm^{-2} and to avoid significant surface damage. The low-energy sputtering for depth-profiling was performed using a 1 keV Ar^+ beam bombardment at 59°. The sputtered area was 1.5 × 1.5 mm^2.

High resolution imaging and Pt and Pd elemental mapping were performed using a Hitachi HD-2300 STEM (scanning transmission electron microscope) equipped with dual energy-dispersive X-ray spectroscopy (EDS) detectors. Data were obtained in the high-angle annular dark-field (HAADF) mode using an accelerating voltage of 200 keV. Cross-sectional samples for such analysis were obtained following an established lift-out procedure[19] using a FEI Helios Nanolab 600 dual-beam focused ion beam (FIB) instrument. Around 1.5 μm of a Pt/C protection layer was deposited on top of

the bilayer film to prevent surface erosion during milling, which was performed using 30 keV Ga^+ ion with 21 nA–93 pA current. In the final step, the surfaces of the extracted samples were cleaned with 2–5 keV and 28–46 pA Ga^+ ion current.

Electrochemical impedance spectroscopy (EIS) was performed using a Solartron analytical 1260 frequency response analyzer in a pseudo-four-probe configuration. A 20 mV perturbation voltage about zero bias was applied over a frequency range of 100 kHz–0.1 Hz. The impedance spectra were insensitive to the gas flow rate in the range used for the measurement, ensuring that the results were not impacted by gas-phase mass diffusion limitations. Electrode resistance values were obtained by fitting the impedance spectra using ZView software (Scribner Associates) with an empirical equivalent circuit comprised of R-CPE circuits, where CPE is a constant phase element.[20] Between 3 and 6 distinct cells were measured for each electrode thickness, and the data in this work reflect averaged values from the multiple cells.

See supplementary material for additional experiment results and discussion.

This research was supported by the Kwanjeong Educational Foundation and the U.S. Department of Energy, through ARPA-e Contract Nos. DE-AR0000495 and DE-AR0000813. This work utilized Micro/Nano Fabrication Facility (NUFAB), NUANCE Center (EPIC and Keck-II), and J. B. Cohen Diffraction X-ray Diffraction Facility at Northwestern University, which are all supported by the Soft and Hybrid Nanotechnology Experimental (SHyNE) Resource (No. NSF ECCS-1542205) and MRSEC program of the National Science Foundation (No. DMR-1720139) at the Materials Research Center. We thank Xin Xu and Kaiting Li for assistance with sample preparation.

REFERENCES

[1] S. M. Haile, D. A. Boysen, C. R. I. Chisholm, and R. B. Merle, Nature **410**, 910 (2001).
[2] S. M. Haile, C. R. Chisholm, K. Sasaki, D. A. Boysen, and T. Uda, Faraday Discuss. **134**, 17 (2007).
[3] D. A. Boysen, T. Uda, C. R. I. Chisholm, and S. M. Haile, Science **303**, 68 (2004).
[4] T. Uda and S. M. Haile, Electrochem. Solid-State Lett. **8**, A245 (2005).
[5] C. R. Chisholm, D. A. Boysen, A. B. Papandrew, S. Zecevic, S. Cha, K. A. Sasaki, Á. Varga, K. P. Giapis, and S. M. Haile, Electrochem. Soc. Interface **18**(3), 53 (2009).
[6] A. B. Papandrew, C. R. I. Chisholm, S. K. Zecevic, G. M. Veith, and T. A. Zawodzinski, J. Electrochem. Soc. **160**, F175 (2012).
[7] A. B. Papandrew, S. S. John, and R. A. Elgammal, J. Electrochem. Soc. **163**, F464 (2016).
[8] M. W. Louie, K. Sasaki, and S. Haile, ECS Trans. **13**(28), 57 (2008).
[9] K. A. Sasaki, "Electrochemical characterization of solid acid fuel cell electrodes," Ph.D. thesis, California Institute of Technology, California, United States, 2010.
[10] A. B. Papandrew, D. L. Wilson, N. M. Cantillo, S. Hawks, R. W. Atkinson, G. A. Goenaga, and T. A. Zawodzinski, J. Electrochem. Soc. **161**, F679 (2014).
[11] M. W. Louie and S. M. Haile, Energy Environ. Sci. **4**, 4230 (2011).
[12] K. A. Sasaki, Y. Hao, and S. M. Haile, Phys. Chem. Chem. Phys. **11**, 8349 (2009).
[13] F. P. Lohmann-Richters, B. Abel, and Á. Varga, J. Mater. Chem. A **6**, 2700 (2018).
[14] R. Rego, A. M. Ferraria, A. M. B. do Rego, and M. C. Oliveira, Electrochim. Acta **87**, 73 (2013).
[15] V. S. Thoi, R. E. Usiskin, and S. M. Haile, Chem. Sci. **6**, 1570 (2015).
[16] H. Okamoto, "Pd-Pt (palladium-platinum)," in *Binary Alloy Phase Diagrams*, 2nd ed., edited by T. B. Massalski, H. Okamoto, P. R. Subramanian, and L. Kacprzak (ASM International, 1990), pp. 3033–3034.
[17] D. Manova, J. W. Gerlach, and S. Mändl, Materials **3**, 4109 (2010).
[18] M. A. Nicolet, Thin Solid Films **52**, 415 (1978).
[19] M. K. Miller, K. F. Russell, K. Thompson, R. Alvis, and D. J. Larson, Microsc. Microanal. **13**, 428 (2007).
[20] M. E. Orazem and B. Tribollet, *Electrochemical Impedance Spectroscopy* (John Wiley & Sons, Inc., Hoboken, NJ, USA, 2008), pp. 1–523.